

Understanding Quantum Weak Values: Basics and Applications

Justin Dressel,¹ Mehul Malik,² Filippo M. Miatto,³ Andrew N. Jordan,^{1,4} and Robert W. Boyd^{2,3}

¹*Department of Physics and Astronomy and Rochester Theory Center,
University of Rochester, Rochester, New York 14627, USA*

²*The Institute of Optics, University of Rochester, Rochester, New York 14627, USA*

³*Department of Physics, University of Ottawa, Ottawa, Ontario, Canada*

⁴*Institute of Quantum Studies, Chapman University, 1 University Drive, Orange, CA 92866, USA*

(Dated: May 19, 2022)

Since its introduction 25 years ago, the quantum weak value has gradually transitioned from a theoretical curiosity to a practical laboratory tool. While its utility is apparent in the recent explosion of weak value experiments, its interpretation has historically been a subject of confusion. Here, we present a pragmatic introduction to the weak value in terms of measurable quantities and explain how it can be determined in the laboratory. Further, we review its application to three distinct experimental techniques. First, as a large interaction parameter it can amplify small signals above technical background noise. Second, as a measurable complex value it enables novel techniques for quantum state tomography and geometric phase determination. Third, as a conditioned average of generalised observable eigenvalues it provides a measurable window into nonclassical features of quantum mechanics. In this selective review, we use a single experimental configuration to discuss and clarify each of these applications.

INTRODUCTION

Postulated in 1988 by Aharonov, Albert, and Vaidman [1] as a “new kind of value for a quantum variable” that appears when averaging pre- and post-selected weak measurements, the quantum weak value has had an extensive and colorful theoretical history [2–4]. Recently, however, the weak value has stepped into a more public spotlight due to three types of experimental applications. It is our aim in this brief and selective tutorial to clarify these three pragmatic roles of the weak value in experiments.

First, in its role as an evolution parameter, a large weak value can help to amplify a detector signal and enable the sensitive estimation of unknown small evolution parameters, such as beam deflection, phase shifts, frequency shifts, temporal shifts, and even temperature shifts [5–14]. Paradigmatic optical experiments that have used this technique include the measurement of 1Å resolution beam displacements due to the quantum spin Hall effect of light “without the need for vibration or air-fluctuation isolation” [5], an angular mirror rotation of 400rad due to linear piezo motion of 14fm using only 63μW of power post-selected from 3.5mW total beam power [6], and a frequency sensitivity of 129kHz/√Hz obtained with 85μW of power post-selected from 2mW total beam power [7]. All these results were obtained in modest tabletop laboratory conditions, which was possible since the technique amplifies the signal above any technical noise background possessing long temporal correlations (e.g., electronic 1/f noise or vibration noise) [15, 16].

Second, in its role as a complex number whose real and imaginary parts can both be measured, the weak value has encouraged new methods for quantum state tomography [17–19] and geometric phase determination [20, 21].

These methods express abstract theoretical quantities such as a quantum state in terms of complex weak values, which can then be determined experimentally. Notably, the real and imaginary components of a quantum state in a particular basis can be directly determined with minimal post-processing using this technique.

Third, in its role as a conditioned average of generalised observable eigenvalues the real part of the weak value has provided a measurable window into nonclassical features of quantum mechanics. Conditioned averages outside the normal eigenvalue range have been linked to paradoxes such as Hardy’s paradox [22, 23] and the three-box paradox [24], as well as the violation of generalised Leggett-Garg inequalities that indicate nonclassical behavior [25–28]. Conditioned averages have also been used to experimentally measure physically meaningful quantities including super-luminal group velocities in optical fiber [29], momentum-disturbance relationships in a two-slit interferometer [30], and locally averaged momentum streamlines (along the energy-momentum tensor field [31]) passing through a two-slit interferometer [32].

This review paper is structured as follows. In the next two sections we explain what a weak value is and how it appears in the theory quite generally. We then explain how it is possible to measure both its real and imaginary parts and explore the three classes of experiments outlined above that make use of weak values. This approach allows us to address the importance and utility of weak values in a clear and direct way without stumbling over interpretations that have historically tended to obscure these points. Throughout this review, we make use of *one* simple notation for expressing theoretical notions, and *one* experimental setup — a polarised beam passing through a birefringent crystal.

WHAT IS A WEAK VALUE?

First introduced in [1], weak values are complex numbers that one can assign to the powers of a quantum observable operator \hat{A} using *two* states: an initial state $|i\rangle$, called the *preparation* or *pre-selection*, and a final state $|f\rangle$, called the *post-selection*. The n^{th} order weak value of \hat{A} has the form

$$A_w^n = \frac{\langle f|\hat{A}^n|i\rangle}{\langle f|i\rangle} \quad (1)$$

where the order n corresponds to the power of \hat{A} that appears in the expression. In this review, we wish to clarify how these peculiar complex expressions appear naturally in laboratory measurements. To accomplish this goal, we derive them in terms of measurable detection probabilities. Weak values of every order appear when we characterise how an intermediate interaction affects these detection probabilities.

Consider a standard prepare-and-measure experiment. If a quantum system is prepared in an initial state $|i\rangle$, the probability of detecting an event corresponding to the final state $|f\rangle$ is given by the squared modulus of their overlap, $P = |\langle f|i\rangle|^2$. If, however, the initial state is modified by an intermediate unitary interaction $\hat{U}(\epsilon)$, the detection probability also changes to $P_\epsilon = |\langle f|i'\rangle|^2 = |\langle f|\hat{U}(\epsilon)|i\rangle|^2$.

In order to calculate the relative change between the original and the modified probability, we must examine the unitary operator $\hat{U}(\epsilon)$ carefully. In quantum mechanics, any observable quantity is represented by a Hermitian operator. Stone's theorem states that any such Hermitian operator \hat{A} can *generate* a continuous transformation along a complementary parameter ϵ via the unitary operator $\hat{U}(\epsilon) = \exp(-i\epsilon\hat{A})$. For instance, if \hat{A} is an angular momentum operator, the unitary transformation generates rotations through an angle ϵ , or if \hat{A} is a Hamiltonian, the unitary operator generates translations along a time interval ϵ , and so on.

If ϵ is small enough—or in other words if $\hat{U}(\epsilon)$ is “weak”—we can consider its Taylor series expansion. The detection probability introduced above can then be written as (shown here to first order):

$$\begin{aligned} P_\epsilon &= |\langle f|\hat{U}(\epsilon)|i\rangle|^2 = |\langle f|(1 - i\epsilon\hat{A} + \dots)|i\rangle|^2 \\ &= P + 2\epsilon \text{Im}\langle i|f\rangle\langle f|\hat{A}|i\rangle + O(\epsilon^2). \end{aligned} \quad (2)$$

As long as $|i\rangle$ and $|f\rangle$ are not orthogonal (i.e. $P \neq 0$), we can divide both sides of Eq. (2) by P to obtain the *relative* correction (shown here to second order):

$$\frac{P_\epsilon}{P} = 1 + 2\epsilon \text{Im}A_w - \epsilon^2 [\text{Re}A_w^2 - |A_w|^2] + O(\epsilon^3), \quad (3)$$

where A_w is the first order weak value and A_w^2 is the second order weak value as defined above in Eq. (1).

Here, we arrive at our operational definition: weak values characterise the relative correction to a detection probability $|\langle f|i\rangle|^2$ due to a small intermediate perturbation $\hat{U}(\epsilon)$ that results in a modified detection probability $|\langle f|\hat{U}(\epsilon)|i\rangle|^2$. Although we show the expansion only to second order here, we emphasise that the full Taylor series expansion for P_ϵ/P is *completely* characterised by complex weak values A_w^n of all orders n .

Terms in the expansion (3) higher than first order can be neglected under two conditions: (a) $2\epsilon \text{Im}A_w$ is sufficiently small compared to P , and (b) P itself is nonzero. Under these conditions, one has a linear relationship between the probability correction and the weak value, which we call the *weak interaction regime*. When these conditions do not hold, the terms involving higher order weak values A_w^n become significant and can no longer be neglected. Most experimental work involving weak values has been done in the weak interaction regime characterised by the first order weak value, and we will limit our discussion to that regime as well. In the next section, we put these ideas in the context of a real optics experiment and discuss how one measures weak values in the lab.

HOW DOES ONE MEASURE A WEAK VALUE?

In general, weak values are complex quantities. In order to determine a weak value, one must be able to measure both its real and imaginary parts. Here, we use an optical experimental example to show how one can measure a complex weak value associated with a polarisation observable. Although this particular example can also be understood using classical wave mechanics (e.g., [33]), the quantum mechanical analysis we provide here has wider applicability.

Consider the setup shown in Fig. 1a. A collimated laser beam is prepared in an initial state $|i\rangle|\psi_i\rangle$, where $|i\rangle$ is an initial polarisation state and $|\psi_i\rangle$ is the state of the transverse beam profile. The polarisation is prepared through the use of a quarter-wave plate (QWP) and a half-wave plate (HWP). The beam then passes through a linear polariser aligned to a final polarisation state $|f\rangle$ before impacting a CCD camera. Each pixel of the CCD measures a photon of this beam with a detection probability given by

$$P = |\langle f|i\rangle|^2 |\langle \psi_f|\psi_i\rangle|^2, \quad (4)$$

where $|\psi_f\rangle$ is the final transverse state postselected by *each pixel*. For our purposes, this state corresponds either to a specific transverse position $|\psi_f\rangle = |x\rangle$ or transverse momentum $|\psi_f\rangle = |p\rangle$, depending on whether we image the position or the momentum space onto the CCD (e.g., using a Fourier lens as shown in Fig. 1c). We will refer to this detection probability P as the “unperturbed” probability.

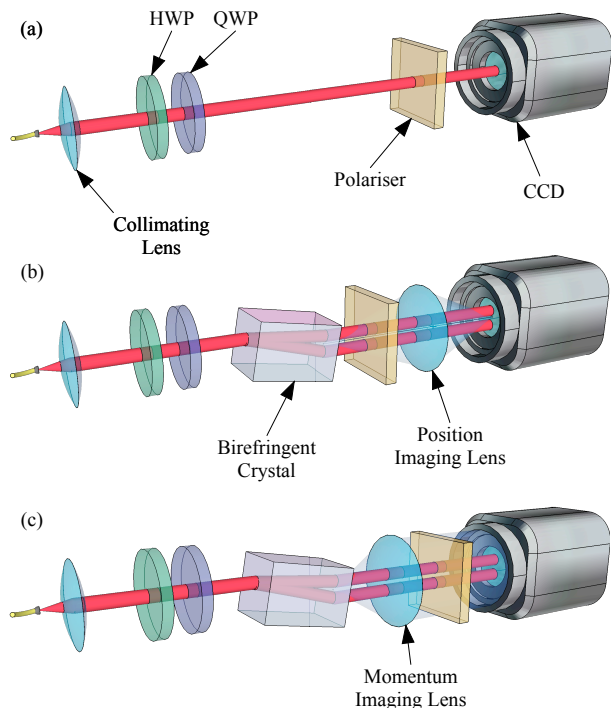


FIG. 1. An experiment for illustrating how one can measure a weak values. (a) A Gaussian beam from a single mode fiber is collimated by a lens and prepared in an initial polarisation state by a quarter-wave plate (QWP) and half-wave plate (HWP). A polariser post-selects the beam on a final polarisation state. A CCD then measures the position-dependent beam intensity. (b) A birefringent crystal is inserted between the wave plates and polariser to displace different polarisations by a small amount. A lens images the transverse position on the output face of the crystal onto the CCD in order to measure the real part of the polarisation weak value as a linear shift in the post-selected intensity. (c) The lens is changed to imaging the far-field of the crystal face onto the CCD as the transverse momentum in order to determine the imaginary part of the polarisation weak value (details in the text).

Now let's introduce a birefringent crystal between the preparation wave plates and the post-selection polariser, as shown in Fig. 1b. The crystal separates the beam into two beams with horizontal and vertical polarisations. The transverse displacements depend on the birefringence properties of the crystal and on the crystal length. Let us assume that the crystal is tilted with respect to the incident beam so that each polarisation component is displaced by an equal amount $\epsilon = \tau v$ where τ is the time spent inside the crystal and v is the displacement speed.

The effect of the birefringent crystal can be expressed by a time evolution operator $\hat{U}(\tau) = e^{-i\tau\hat{H}/\hbar}$ with an

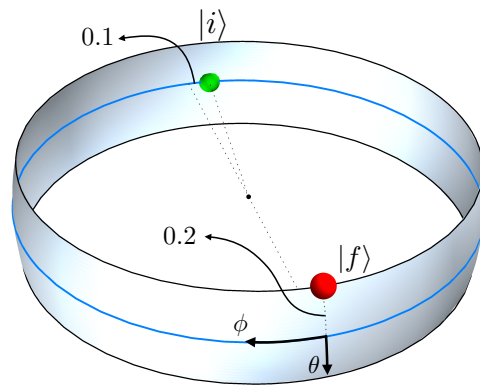


FIG. 2. A band around the equator of the Poincaré sphere showing the initial polarisation $|i\rangle$ (green dot, back of sphere) from Eq. 8 and post-selection polarisation $|f\rangle$ (red dot, front of sphere) from Eq. 9. We also indicate the small angles that make $|f\rangle$ almost orthogonal to $|i\rangle$.

effective interaction Hamiltonian

$$\hat{H} = v\hat{S} \otimes \hat{p}. \quad (5)$$

Here, $\hat{S} = |H\rangle\langle H| - |V\rangle\langle V|$ is the Stokes polarisation operator that assigns eigenvalues $+1$ and -1 to the $|H\rangle$ and $|V\rangle$ polarisations respectively, and \hat{p} is the transverse momentum operator that generates translations in the transverse position x . This time evolution operator $\hat{U}(\tau)$ correlates the polarisation components of the beam with their transverse position by translating them in opposite directions. Each pixel of the CCD then collects a photon with a “perturbed” probability given by

$$P_\epsilon = |\langle f | \langle \psi_f | e^{-i\epsilon\hat{S} \otimes \hat{p}/\hbar} | i \rangle | \psi_i \rangle|^2 \quad (6)$$

which has the form of Eq. (2) with the generic operator \hat{A} replaced by the product operator $\hat{S} \otimes \hat{p}$.

As a visual example, consider a Gaussian beam

$$\langle x | \psi_i \rangle = (2\pi\sigma^2)^{-1/4} \exp\left(-\frac{x^2}{4\sigma^2}\right), \quad (7)$$

with an initial antidiagonal polarisation preparation with a slight ellipticity:

$$|i\rangle = \frac{|H\rangle - e^{i\phi}|V\rangle}{\sqrt{2}}, \quad \phi = 0.1 \quad (8)$$

that passes through a linear post-selection polariser that is oriented at a small angle (0.2 rad in this example) from the diagonal state:

$$|f\rangle = \cos\frac{\theta}{2}|H\rangle + \sin\frac{\theta}{2}|V\rangle, \quad \theta = \frac{\pi}{2} - 0.2. \quad (9)$$

These two nearly orthogonal polarisation states are shown on a band around the equator of the Poincaré

sphere in Fig. 2. Without the crystal present (Fig. 1a), the CCD measures the initial Gaussian intensity profile shown as a dashed line on the left of Fig. 3 with a total post-selection probability given by $|\langle f|i \rangle|^2 = 0.012$. When the crystal is present (Fig. 1b), the orthogonal polarisation components become spatially separated by a displacement ϵ before passing through the post-selection polariser. The measured profiles for different crystal lengths are shown as the solid red line distributions on the left of Fig. 3. The dotted blue line distributions show the unperturbed profiles for comparison.

In the weak interaction regime, the crystal is short, ϵ is small, and the two orthogonally polarised beams are displaced by a small amount before they interfere at the post-selection polariser. As shown in the last section, we can expand the ratio between the perturbed and unperturbed probabilities to first order in ϵ and isolate the linear probability correction term:

$$\begin{aligned} \frac{P_\epsilon}{P} - 1 &\approx \frac{2\tau}{\hbar} \text{Im}H_w \\ &= \frac{2\epsilon}{\hbar} [\text{Re}S_w \text{Im}p_w + \text{Im}S_w \text{Re}p_w]. \end{aligned} \quad (10)$$

Since the Hamiltonian from Eq. (5) is of product form, its first order weak value contribution $\text{Im}H_w$ expands to a symmetric combination of the real and imaginary parts of the weak values of polarisation $S_w = \langle f|\hat{S}|i \rangle / \langle f|i \rangle$ and momentum $p_w = \langle \psi_f|\hat{p}|\psi_i \rangle / \langle \psi_f|\psi_i \rangle$. A clever choice of pre- and post-selection states therefore allows an experimenter to isolate each of these quantities using different experimental setups.

To illustrate this idea for the polarisation weak value, the procedure for measuring the real part $\text{Re}S_w$ is shown in Fig. 1b. We image the output face of the crystal onto the CCD so that each pixel corresponds to a post-selection of the transverse position $|\psi_f\rangle = |x\rangle$. As a result, the momentum weak value for each pixel becomes

$$p_w = \frac{\langle x|\hat{p}|\psi_i \rangle}{\langle x|\psi_i \rangle} = \frac{-i\hbar\partial_x\psi_i(x)}{\psi_i(x)} = i\hbar\frac{x}{2\sigma^2}. \quad (11)$$

Since this expression is purely imaginary, Eq. (10) simplifies to

$$\frac{P_\epsilon}{P} \approx 1 + \epsilon \frac{x}{\sigma^2} \text{Re}S_w, \quad (12)$$

effectively isolating the quantity $\text{Re}S_w$ to first order in ϵ . The solid green curves on the right of Fig. 3 illustrate the ratio P_ϵ/P as a function of x for different values of ϵ . When ϵ is sufficiently small, the expansion of P_ϵ/P to first order in Eq. (12) (dashed black lines on the right of Fig. 3) is a good approximation over most of the beam profile.

The analogous procedure for measuring the imaginary part $\text{Im}S_w$ is shown in Fig. 1c. We image the Fourier plane of the crystal onto the CCD so that each pixel corresponds to a post-selection of the transverse momentum

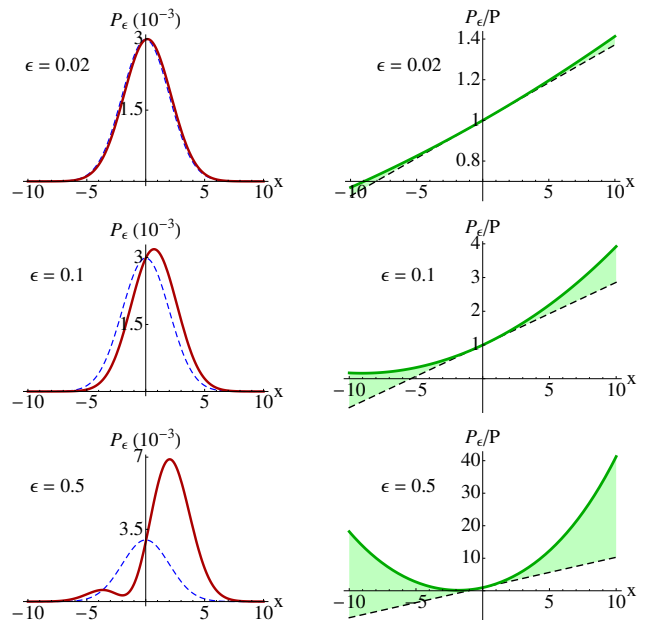


FIG. 3. (left) Unperturbed (dashed blue) and perturbed (solid red) profiles measured by the CCD for several crystal lengths producing beam displacements ϵ . (right) The ratio of the perturbed to the unperturbed profiles (solid green) compared to the first order approximation (dashed black) described in Eq. (12). When ϵ is sufficiently small the first order approximation adequately models the change over most of the profile.

$|\psi_f\rangle = |p\rangle$. As a result, the momentum weak value for each pixel becomes simply

$$p_w = \frac{\langle p|\hat{p}|\psi_i \rangle}{\langle p|\psi_i \rangle} = \frac{p\langle p|\psi_i \rangle}{\langle p|\psi_i \rangle} = p. \quad (13)$$

Since this expression is now purely real, Eq. (10) simplifies to

$$\frac{P_\epsilon}{P} \approx 1 + \epsilon \frac{2p}{\hbar} \text{Im}S_w, \quad (14)$$

effectively isolating the quantity $\text{Im}S_w$ to first order in ϵ .

Note that we could also isolate the real and imaginary parts of p_w in a similar manner through a judicious choice of polarisation post-selection states. More generally, one can use this technique to isolate weak values of any desired observable by constructing Hamiltonians in a product form like (5) and cleverly choosing the pre- and post-selection of the auxiliary degree of freedom.

HOW CAN WEAK VALUES BE USEFUL?

In the previous section, we showed how the relative change in post-selection probability can be completely described by complex weak value parameters. We also elucidated how the real and imaginary parts of the first

order weak value can be isolated and therefore measured in the weak interaction regime.

In this section we focus on three main applications of the first order weak value. First, we show how clever choices of the initial and final post-selected states can result in large weak values that can be used to sensitively determine unknown parameters affecting the state evolution. Second, we show how the complex character of the weak value may be used to directly determine a quantum state. Third, we show how the real part of the weak value may be interpreted as a form of conditioned average pertaining to an observable.

Weak value amplification

In precision metrology an experimenter is interested in estimating a small interaction parameter, such as the transverse beam displacement $\epsilon = \tau v$ due to the crystal in the previous section. As the first order approximation of P/P_ϵ holds in the weak interaction regime, the value of ϵ can be directly determined. We briefly note that the appearance of the joint weak value of Eq. (10) in a parameter estimation experiment is no accident—as pointed out in [34], this quantity is the *score* used to calculate the Fisher information that determines the Cramer-Rao bound for the estimation of an unknown parameter like ϵ [35, 36].

Being able to resolve a small ϵ in the presence of background noise requires the joint weak value factor in Eq. (10) to be sufficiently large. When this weak value factor is large it will *amplify* the linear response. Critically, the initial and final states for the weak values S_w and p_w can be strategically chosen to produce a large amplification factor. This is the essence of the technique used in *weak value amplification* experiments such as [5–14].

For a tangible example of how this amplification works for estimating ϵ , consider the measurement in Fig. 1b of the previous section. Averaging the position recorded at every pixel produces the centroid

$$\int x P_\epsilon(x|\theta) dx \approx \frac{\langle x \rangle + \epsilon(\langle x^2 \rangle / \sigma^2) \text{Re}S_w}{1 + \epsilon(\langle x \rangle / \sigma^2) \text{Re}S_w}, \quad (15)$$

$$= \epsilon \text{Re}S_w.$$

To compute this expression we used the perturbed conditional probability $P_\epsilon(x|\theta) = P_\epsilon(x, \theta) / \int P_\epsilon(x, \theta) dx$ computed from Eq. (12) as a function of the pixel position x , and a given post-selection polarisation angle θ , as well as the Gaussian moments $\langle x \rangle = 0$ and $\langle x^2 \rangle = \sigma^2$ of the unperturbed beam profile. Dividing the measured centroid by the (known) quantity $\text{Re}S_w$ allows us to determine the small parameter ϵ .

Alternatively, if the CCD measures the Fourier plane as in Fig. 1c, then each pixel corresponds to a transverse

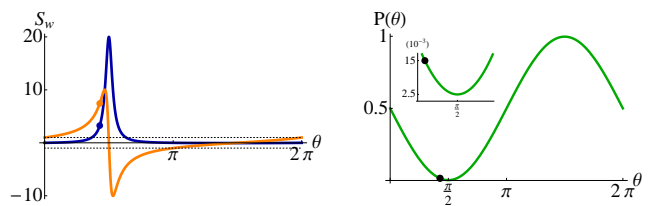


FIG. 4. (left) Real (orange) and imaginary (blue) parts of the polarisation weak value $S_w = \langle f|\hat{S}|i\rangle/\langle f|i\rangle$, with initial state $|i\rangle$ given in Eq. 8 and shown in Fig. 2, and final state $|f\rangle$ that depends on a varying angle θ . The eigenvalue bounds of ± 1 are shown as dotted lines for reference. (right) The post-selection probability $P(\theta) = |\langle f|i\rangle|^2$ as a function of θ , showing how a large weak value corresponds to a small detection probability. The inset shows the small probability region enlarged for clarity.

momentum. Finding the centroid in this case produces

$$\int p P_\epsilon(p|\theta) dp \approx \frac{\langle p \rangle + 2\epsilon \langle p^2 \rangle \text{Im}S_w/\hbar}{1 + 2\epsilon \langle p \rangle \text{Im}S_w/\hbar} \quad (16)$$

$$= \epsilon \frac{\hbar}{2\sigma^2} \text{Im}S_w,$$

where we have used Eq. (14) and the Gaussian moments $\langle p \rangle = 0$ and $\langle p^2 \rangle = (\hbar/2\sigma)^2$ of the unperturbed beam profile.

The amplification occurs in each case because the factor $\text{Re}S_w$ in (15) or $2\langle p^2 \rangle \text{Im}S_w$ in (16) can be made large by clever choices of polarisation post-selection. For our example states (Eqs. (8) and (9)), the polarisation weak value is $S_w = \langle f|\hat{S}|i\rangle/\langle f|i\rangle \approx 7.5 + 3.2i$. Notably, both the real and imaginary parts of the weak value in this case are larger than 1, which is the maximum eigenvalue of \hat{S} . The left plot in Fig. 4 shows how the real and imaginary parts of the weak value vary with the choice of post-selection angle θ .

There is no free lunch for obtaining such amplification, however. As the weak value factor S_w becomes large, the detection probability necessarily decreases, as shown in the right plot of Fig. 4. Hence, the weak interaction approximation that assumes $2\epsilon \text{Im}(S \otimes p)_w \ll |\langle f|i\rangle|^2 |\langle \psi_f|\psi_i\rangle|^2$ for each pixel will eventually break down and it will be necessary to include higher-order terms in ϵ that have been neglected, spoiling the linear response [3, 37–50]. Moreover, the resulting low detection rate will lead to increased collection times needed to overcome the noise floor. Indeed, a careful analysis shows that the signal-to-noise ratio for determining ϵ within a fixed time duration remains constant as the amplification increases [15, 16]—the signal gained by increasing the amplification factors in (15) or (16) will exactly cancel the uncorrelated shot noise gained by decreasing the detection rate.

Nevertheless, there are two distinct advantages to us-

ing this amplification technique: 1) the detector only needs to collect a fraction of the total beam power due to the post-selection polariser, and 2) the amplification is robust against additional technical noise that possesses long temporal correlations (such as $1/f$ noise) [15, 16]. The former advantage allows less expensive equipment to be used, while simultaneously enabling the uncollected beam power to be redirected elsewhere for other purposes. The latter advantage allows one to amplify the signal without also amplifying unrelated (but common) technical noise backgrounds. These two advantages combined are precisely what has permitted experiments such as [5–14] to achieve such phenomenal precision with relatively modest laboratory equipment.

Measurable complex value

Since weak values are measurable complex quantities, they can be used to directly measure other normally inaccessible complex quantities in the quantum theory that can be expanded into sums and products of complex weak values. Most notably, one can “directly” measure the quantum state itself using this technique [17–21]. Conventionally, a quantum state is determined through the indirect process of quantum tomography [51]. Like its classical counterpart, quantum tomography involves making a series of projective measurements in different bases of a quantum state. This process is indirect in that it involves a time consuming post-processing step where the density matrix of the state must be *globally* reconstructed through a numerical search over the alternatives consistent with the measured projective slices. Propagating experimental error through this reconstruction step can be problematic, and the computation time can be prohibitive for determining high-dimensional quantum states, such as those of orbital angular momentum.

We can bypass the need for such a global reconstruction step by expanding individual components of a quantum state directly in terms of measurable weak values. For a simple example, let us determine the complex components of the initial polarisation state $|i\rangle$ of our example, expanded in the weak measurement basis $\{|H\rangle, |V\rangle\}$. This is accomplished by the insertion of the identity and multiplication by a strategically chosen constant factor $c = \langle D|H\rangle/\langle D|i\rangle = \langle D|V\rangle/\langle D|i\rangle$, where the post-selection state $|D\rangle$ is unbiased with respect to both $|H\rangle$ and $|V\rangle$. With this clever choice the scaled state has the form

$$c|i\rangle = \underbrace{\frac{\langle D|H\rangle\langle H|i\rangle}{\langle D|i\rangle}}_{H_w}|H\rangle + \underbrace{\frac{\langle D|V\rangle\langle V|i\rangle}{\langle D|i\rangle}}_{V_w}|V\rangle. \quad (17)$$

That is, each complex component of the scaled state $c|i\rangle$ can be directly measured as a complex first order weak

value. After determining these complex components experimentally, the state can be subsequently renormalised to eliminate the constant c up to a global phase.

Furthermore, we can write the projections as $|H\rangle\langle H| = (\hat{1} + \hat{S})/2$ and $|V\rangle\langle V| = (\hat{1} - \hat{S})/2$, so we can rewrite the required weak values $H_w = (1 + S_w)/2$ and $V_w = (1 - S_w)/2$ in terms of the single polarisation weak value S_w . We showed earlier how to isolate and measure both the real and imaginary parts of this polarisation weak value. Thus, we can completely determine the state $|i\rangle$ after the polarisation weak value S_w has been measured using the special post-selection $|D\rangle$.

The primary benefit of this tomographic approach is that minimal post-processing—and thus minimal experimental error propagation—is required to reconstruct individual state components from the experimental data. The real and imaginary parts of each state component directly appear in the linear response of a measurement device up to appropriate scaling factors. The downside of this approach is that the denominator $\langle D|i\rangle$ in the constant c cannot become too small or the linear approximation used to measure S_w will break down [52]. This restriction limits the generality of the technique for faithfully determining a truly unknown $|i\rangle$. Nevertheless, the technique can be useful for determining the components of most pure states [17]. To handle mixed states the post-selection must be scanned across a mutually unbiased basis, which will determine the Dirac distribution for the state instead [18, 19]; this distribution is related to the density matrix via a Fourier transform.

Conditioned average

As our final example of the utility of weak values, we show that the *real* part of a weak value can be interpreted as a form of conditioned average associated with an observable. To show this we first consider how each pixel records polarization information in the absence of post-selection. After summing over all complementary post-selections $|f\rangle$ in the perturbed probability $P_\epsilon(x, f)$ in Eq. (6), we can express the total perturbed pixel probability as

$$P_\epsilon(x) = \sum_f |\langle f|\langle x|e^{-i\epsilon\hat{S}\otimes\hat{p}/\hbar}|i\rangle|\psi_i\rangle|^2 = \langle i|\hat{P}_x|i\rangle, \quad (18)$$

in terms of a probability operator $\hat{P}_x = |\langle x - \epsilon\hat{S}|\psi_i\rangle|^2$. This operator indicates that the crystal interaction shifts the initial profile $|\langle x|\psi_i\rangle|^2$ of the beam by an amount proportional to the polarisation.

An experimenter can then *assign* a value of (x/ϵ) to each pixel x and average those values over the perturbed profile in (18) to obtain the average polarisation

$$\int \frac{x}{\epsilon} P_\epsilon(x) dx = \langle i|\hat{S}|i\rangle \quad (19)$$

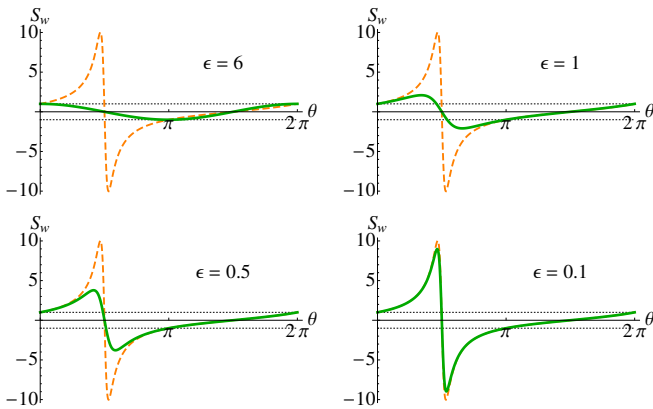


FIG. 5. Conditioned average (20) of generalised polarisation eigenvalues x/ϵ for various values of the crystal length ϵ , using the beam profile illustrated in Figure 2. For large ϵ the average is a classical conditioned average constrained to the eigenvalue range (black dotted lines). For sufficiently small ϵ , however, the conditioned average (green, solid) approximates the real part (orange, dashed) of the polarisation weak value in Figure 4.

for *any* preparation state $|i\rangle$. The values (x/ϵ) assigned to each pixel act as *generalised eigenvalues* for the polarisation operator \hat{S} [53–55]. An experimenter must assign these values in place of the standard polarisation eigenvalues of ± 1 because the pixels are only weakly correlated with the polarisation. Although the values (x/ϵ) generally lie well outside the eigenvalue range of \hat{S} , their experimental average in Eq. (19) always produces a sensible average polarization.

Including the post-selection polariser $|f\rangle$ changes this result. The polariser conditions the total pixel probability of Eq. (18). After assigning the same generalised polarization eigenvalues x/ϵ to each pixel and averaging these values over the conditioned profile, an experimenter will find the *conditioned average*

$$\int \frac{x}{\epsilon} P_\epsilon(x|f) dx = \text{Re} \frac{\langle f|\hat{S}|i\rangle}{\langle f|i\rangle} + O(\epsilon^2). \quad (20)$$

As we already showed in Eq. (15) this conditioned average of generalized polarization eigenvalues approximates the *real part* of a weak value for small ϵ in an experimentally meaningful way.

Importantly, even when ϵ is not small the full conditioned average of generalised eigenvalues (20) will smoothly interpolate between the weak value approximation and a *classical conditioned average* of polarisation. In Fig. 5 we illustrate this interpolation for different values of ϵ . This smooth correspondence is essential for associating the experimental average Eq. (20) to the polarisation \hat{S} in any meaningful way. Indeed, several of the authors (JD and ANJ) showed in [50] that this interpolation exactly describes how the initial polarisation state *deco-*

heres into a classical polarisation state with increasing measurement strength. Moreover, this technique of constructing conditioned averages of generalised eigenvalues works quite generally for other detectors [26, 27, 56, 57] and produces similar interpolations between a classical conditioned average and the real part of a weak value.

The link between weak values and conditioned averages has been used to address several quantum paradoxes, such as Hardy’s paradox [22, 23] and the three-box paradox [24]. Anomalously large weak values provide a *measurable* window into the inner workings of these paradoxes by indicating when quantum observables cannot be understood in any classical way as properties related to their eigenvalues. Similarly, anomalously large weak values have been linked to violations of generalised Leggett-Garg inequalities [25–28, 58] that indicate nonclassical behavior in measurement sequences. This link has also been exploited to provide an experimental method for determining physically meaningful conditioned quantities, such as group velocities in optical fiber [29], or the momentum-disturbance relationships for a two-slit interferometer [30].

A particularly notable experimental demonstration of the connection between weak values and physically meaningful conditioned averages is the measurement of the locally averaged momentum streamlines $p_B(x)$ passing through a two-slit interferometer performed by Kocsis *et al.* [32] using the weak value identity

$$\text{Re} \frac{\langle x|\hat{p}|\psi_i\rangle}{\langle x|\psi_i\rangle} = \partial_x \Phi(x) = p_B(x), \quad (21)$$

where $\langle x|\psi_i\rangle = |\langle x|\psi_i\rangle| \exp(i\Phi(x)/\hbar)$ is the polar decomposition of the initial transverse profile. This phase gradient has appeared historically in Madelung’s hydrodynamic approach to quantum mechanics [59, 60], Bohm’s causal model [61, 62], and even the momentum part of the local energy-momentum tensor [31]. Importantly, the weak value connection provides this quantity with an experimentally meaningful definition as a conditioned average.

CONCLUSIONS

In this tutorial we reviewed how the quantum weak value naturally appears in laboratory situations. We operationally defined weak values as complex parameters that completely characterise the relative corrections to detection probabilities that are caused by an intermediate interaction. When the interaction is sufficiently weak, these relative corrections can be well approximated by first order weak values.

Using an optical example of a polarised beam passing through a birefringent crystal, we showed how to use a product interaction to isolate and measure both the real

and imaginary parts of first order weak values. This example allowed us to discuss three distinct roles that the first order weak value has played in recent experiments.

First, we showed how a large weak value can be used to amplify a signal used to sensitively estimate an unknown interaction parameter in the (linear) weak interaction regime. Although the signal-to-noise ratio remains constant from this amplification due to a corresponding reduction in detection probability, the technique allows one to amplify the signal above other technical noise backgrounds using fairly modest laboratory equipment.

Second, we showed that since the first order weak value is a measurable complex parameter, it can be used to experimentally determine other complex theoretical quantities. Notably, we showed how the components of a pure quantum state may be directly determined up to a global phase by measuring carefully chosen weak values.

Third, we carefully discussed the relationship between the real part of a first order weak value and a conditioned average for an observable. By conditionally averaging generalised eigenvalues for the observable, we showed that one obtains an average that smoothly interpolates between a classical conditioned average and a weak value as the interaction strength changes.

We have emphasised the generality of the quantum weak value as a tool for describing experiments. Due to this generality, we anticipate that many more applications of the weak value will be found in time. We hope this tutorial will encourage further exploration along these lines.

Acknowledgments.—JD and ANJ acknowledge support from the National Science Foundation under Grant No. DMR-0844899, and the US Army Research Office under grant Grant No. W911NF-09-0-01417. MM, FMM, and RWB acknowledge support from the US DARPA InPho program. FMM and RWB acknowledge support from the Canada Excellence Research Chairs Program. The authors thank Jonathan Leach for helpful discussions.

-
- [1] Y. Aharonov, D. Z. Albert, and L. Vaidman, *Phys. Rev. Lett.* **60**, 1351 (1988); I. M. Duck, P. M. Stevenson, and E. C. G. Sudarshan, *Phys. Rev. D* **40**, 2112 (1989); N. W. M. Ritchie, J. G. Story, and R. G. Hulet, *Phys. Rev. Lett.* **66**, 1107 (1991).
- [2] Y. Aharonov and L. Vaidman, *Lect. Notes Phys.* **734**, 399 (2008); Y. Aharonov, S. Popescu, and J. Tollaksen, *Physics Today* **63**, 27 (2010).
- [3] A. G. Kofman, S. Ashkab, and F. Nori, *Phys. Rep.* **520**, 43 (2012).
- [4] Y. Shikano, in *Measurements in Quantum Mechanics*, edited by M. R. Pahlavani (InTech, 2012) Chap. 4, p. 75.
- [5] O. Hosten and P. Kwiat, *Science* **319**, 787 (2008).
- [6] P. B. Dixon, D. J. Starling, A. N. Jordan, and J. C. Howell, *Phys. Rev. Lett.* **102**, 173601 (2009).
- [7] D. J. Starling, P. B. Dixon, A. N. Jordan, and J. C. Howell, *Phys. Rev. A* **82**, 063822 (2010).
- [8] D. J. Starling, P. B. Dixon, N. S. Williams, A. N. Jordan, and J. C. Howell, *Phys. Rev. A* **82**, 011802(R) (2010).
- [9] M. D. Turner, C. A. Hagedorn, S. Schlamminger, and J. H. Gundlach, *Opt. Lett.* **36**, 1479 (2011).
- [10] J. M. Hogan, J. Hammer, S.-W. Chiow, S. Dickerson, D. M. S. Johnson, T. Kovachy, A. Sugarbaker, and M. A. Kasevich, *Opt. Lett.* **36**, 1698 (2011).
- [11] M. Pfeifer and P. Fischer, *Opt. Lett.* **19**, 16508 (2011).
- [12] X. Zhou, Z. Xiao, H. Luo, and S. Wen, *Phys. Rev. A* **85**, 043809 (2012).
- [13] P. Egan and J. A. Stone, *Opt. Lett.* **37**, 4991 (2012).
- [14] G. Strübi and C. Bruder, *Phys. Rev. Lett.* **110**, 083605 (2013).
- [15] D. J. Starling, P. B. Dixon, A. N. Jordan, and J. C. Howell, *Phys. Rev. A* **80**, 041803 (2009).
- [16] A. Feizpour, X. Xingxing, and A. M. Steinberg, *Phys. Rev. Lett.* **107**, 133603 (2011).
- [17] J. S. Lundeen, B. Sutherland, A. Patel, C. Stewart, and C. Bamber, *Nature* **474**, 188 (2011).
- [18] J. S. Lundeen and C. Bamber, *Phys. Rev. Lett.* **108**, 070402 (2012).
- [19] J. Z. Salvail, M. Agnew, A. S. Johnson, E. Bolduc, J. Leach, and R. W. Boyd, “Full characterisation of polarisation states of light via direct measurement,” (2012), arXiv:1206.2618.
- [20] H. Kobayashi, S. Tomate, T. Nakanishi, K. Sugiyama, and M. Kitano, *Phys. Rev. A* **81**, 012104 (2010).
- [21] H. Kobayashi, S. Tomate, T. Nakanishi, K. Sugiyama, and M. Kitano, *J. Phys. Soc. Jpn.* **80**, 034401 (2011).
- [22] J. S. Lundeen and A. M. Steinberg, *Phys. Rev. Lett.* **102**, 020404 (2009).
- [23] K. Yokota, T. Yamamoto, M. Koashi, and N. Imoto, *New J. Phys.* **11**, 033011 (2009).
- [24] K. J. Resch, J. S. Lundeen, and A. M. Steinberg, *Phys. Lett. A* **324**, 125 (2004).
- [25] A. Palacios-Laloy, F. Mallet, F. Nguyen, P. Bertet, D. Vion, D. Esteve, and A. N. Korotkov, *Nature Phys.* **6**, 442 (2010).
- [26] M. E. Goggin, M. P. Almeida, M. Barbieri, B. P. Lanyon, J. L. O’Brien, A. G. White, and G. J. Pryde, *Proc. Natl. Acad. Sci. U. S. A.* **108**, 1256 (2011).
- [27] J. Dressel, C. J. Broadbent, J. C. Howell, and A. N. Jordan, *Phys. Rev. Lett.* **106**, 040402 (2011).
- [28] Y. Suzuki, M. Iinuma, and H. F. Hofmann, *New J. Phys.* **14**, 103022 (2012).
- [29] N. Brunner, V. Scarani, M. Wegmuller, M. Legre, and N. Gisin, *Phys. Rev. Lett.* **93**, 203902 (2004).
- [30] R. Mir, J. S. Lundeen, M. W. Mitchell, A. M. Steinberg, J. L. Garretson, and H. M. Wiseman, *New J. Phys.* **9**, 287 (2007).
- [31] B. J. Hiley and R. Callaghan, *Found. Phys.* **42**, 192 (2012).
- [32] S. Kocsis, B. Braverman, S. Ravets, M. J. Stevens, R. P. Mirin, L. K. Shalm, and A. M. Steinberg, *Science* **332**, 1170 (2011).
- [33] J. C. Howell, D. J. Starling, P. B. Dixon, P. K. Vudyaasetu, and A. N. Jordan, *Phys. Rev. A* **81**, 033813 (2010).
- [34] H. Hofmann, *Phys. Rev. A* **83**, 022106 (2011).
- [35] H. Hofmann, M. E. Goggin, M. P. Almeida, and M. Barbieri, *Phys. Rev. A* **86**, 040102(R) (2012).
- [36] C. W. Helstrom, *Quantum Detection and Estimation Theory* (Academic, New York, 1976).

- [37] T. Geszti, Phys. Rev. A **81**, 044102 (2010).
- [38] Y. Shikano and A. Hosoya, J. Phys. A **43**, 025304 (2010).
- [39] Y.-W. Cho, H.-T. Lim, Y.-S. Ra, and Y.-H. Kim, New J. Phys. **12**, 023036 (2010).
- [40] Y. Shikano and A. Hosoya, Physica E **43**, 776 (2011).
- [41] S. Wu and Y. Li, Phys. Rev. A **83**, 052106 (2011).
- [42] A. D. Parks and J. E. Gray, Phys. Rev. A **84**, 012116 (2011).
- [43] X. Zhu, Y. Zhang, S. Pang, C. Qiao, Q. Liu, and S. Wu, Phys. Rev. A **84**, 052111 (2011).
- [44] T. Koike and S. Tanaka, Phys. Rev. A **84**, 062106 (2011).
- [45] A. Di Lorenzo, Phys. Rev. A **85**, 032106 (2012).
- [46] J. Dressel and A. N. Jordan, Phys. Rev. A **85**, 012107 (2012).
- [47] K. Nakamura, A. Nishizawa, and M.-K. Fujimoto, Phys. Rev. A **85**, 012113 (2012).
- [48] Y. Susa, Y. Shikano, and A. Hosoya, Phys. Rev. A **85**, 052110 (2012).
- [49] A. K. Pan and A. Matzkin, Phys. Rev. A **85**, 022122 (2012).
- [50] J. Dressel and A. N. Jordan, Phys. Rev. Lett. **109**, 230402 (2012).
- [51] J. Altepeter, E. Jeffrey, and P. Kwiat, Adv Atom Mol Opt Phy **52**, 105 (2005).
- [52] E. Haapasalo, P. Lahti, and J. Schultz, Phys. Rev. A **84**, 052107 (2011).
- [53] J. Dressel, S. Agarwal, and A. N. Jordan, Phys. Rev. Lett. **104**, 240401 (2010).
- [54] J. Dressel and A. N. Jordan, J. Phys. A: Math. Theor. **45**, 015304 (2012).
- [55] J. Dressel and A. N. Jordan, Phys. Rev. A **85**, 022123 (2012).
- [56] G. J. Pryde, J. L. O'Brien, A. G. White, T. C. Ralph, and H. M. Wiseman, Phys. Rev. Lett. **94**, 220405 (2005).
- [57] J. Dressel, Y. Choi, and A. N. Jordan, Phys. Rev. B **85**, 045320 (2012).
- [58] N. S. Williams and A. N. Jordan, Phys. Rev. Lett. **100**, 026804 (2008).
- [59] E. Madelung, Naturwissenschaften **14**, 1004 (1926).
- [60] E. Madelung, Z. Phys. **40**, 322 (1927).
- [61] D. Bohm, Phys. Rev. **85**, 166 (1952); **85**, 180 (1952).
- [62] H. M. Wiseman, New J. Phys. **9**, 165 (2007).